3957

INSTITUTE OF PHYSICS PUBLISHING JOURNAL OF PHYSICS: CONDENSED MATTER

J. Phys.: Condens. Matter **14** (2002) R1035–R1062 PII: S0953-8984(02)13612-5

TOPICAL REVIEW

Nonlinear two-dimensional vibrational spectroscopy of peptides

Sander Woutersen[1] **and Peter Hamm**[2]

[1] FOM-Institute for Atomic and Molecular Physics, Kruislaan 407, 1098 SJ Amsterdam, The Netherlands
[2] Universität Zürich, Physikalisch Chemisches Institut, Winterthurerstrasse 190, CH-8057 Zürich, Switzerland

Received 20 June 2002
Published 19 September 2002
Online at stacks.iop.org/JPhysCM/14/R1035

Abstract

In this overview, we discuss theoretical and experimental aspects of nonlinear two-dimensional infrared (2D-IR) spectroscopy. With this technique both peptide conformation and conformational flexibility can be probed. The quantitative relation between the experimental 2D-IR spectrum and the peptide conformation is discussed, and examples of how the conformation of a peptide and the timescale of its fluctuations are derived from its (time-resolved) 2D spectrum are presented.

Contents

0953-8984/02/391035+28$30.00

1. Introduction

Knowledge of the conformations and conformational dynamics of proteins and peptides is essential for understanding their biological functionality. At present, the two most important methods for determining biomolecular conformations are x-ray diffraction (XRD) and nuclear magnetic resonance (NMR) spectroscopy. With x-ray diffraction, the molecular conformation as it occurs in the crystalline phase can be determined with very high spatial resolution. Great progress has been achieved in developing time-resolved x-ray diffraction techniques [1–5], allowing one to directly follow structural changes during photochemical reactions in the crystal environment. In principle, there is no limit to the time resolution of this approach, but due to technical restraints the time resolution is currently limited to a few 100 ps in most published works. In the solution phase, the most powerful technique for elucidating protein and peptide conformations is NMR spectroscopy [6–8]. The most elementary techniques measure the through-bond scalar couplings between proton spins, from which approximate values for the ϕ dihedral angles of the peptide or protein under study can be obtained, and the nuclear Overhauser effect (NOE), which is used to detect through-space dipolar couplings, and from which distances between spins are estimated. The resulting information, together with knowledge of the backbone composition, is generally sufficient to derive the molecular conformation. The through-bond and through-space couplings are usually obtained from two-dimensional NMR spectra, in which the coupling strengths can be read off as the intensity of the off-diagonal peaks [9].

Dynamical changes in the conformation can also be studied with NMR spectroscopy. If the dynamical process is sufficiently slow, the evolution can be followed by measuring NMR spectra in real time [10]. The time resolution achievable in this way will be limited, and although millisecond time resolution has been obtained by combining stopped-flow techniques with NMR [11, 12], it is clear that in general the dynamics should take place on a timescale slow compared to the NMR measurement in order to be observable in real time.

Faster conformational dynamics can be probed indirectly through the spin relaxation processes to which they give rise. Fluctuations in the conformation cause fluctuations in the spin–spin couplings, and hence give rise to different types (NOE cross relaxation, T_1) of relaxation phenomena. The relaxation parameters are related to the spectral density of the conformational fluctuations of the degree of freedom modulating the spin–spin coupling. By measuring the relaxation rates, one obtains the spectral density at the (difference and sum) frequencies of the spin transitions [13]. By varying the external magnetic field strength, one can vary these frequencies, and hence the spectral density of the fluctuations can, in principle, be probed continuously in the accessible frequency range [14]. This range extends to about 1 GHz, corresponding to timescales of 1 ns and slower.

However, in many biomolecular systems a significant part of the dynamics takes place on much faster timescales. An important case are small peptides in solution, which are very flexible, and which strongly interact with the solvent. Such small peptides are considered good model systems for investigating the elementary steps of protein folding (for instance, α-helix formation). Part of the dynamics of these molecules occurs on a (sub)picosecond timescale, which is difficult to access with NMR. It is still possible to derive picosecond time constants from NMR relaxation measurements by fitting correlation functions to the observed spectral densities, but since the experimentally accessible frequencies (<1 GHz) are so low compared to the time constants obtained in this way, the values of the latter depend critically on the functional form assumed for the correlation function [13, 14], and hence should be interpreted with caution. Faster (subpicosecond) fluctuations can essentially not be observed at all with NMR.

Recent work [15–36] has shown that two-dimensional infrared (2D-IR) might be a valuable experimental complement to 2D-NMR for studying fast conformational dynamics. The idea of 2D-IR spectroscopy is to apply the conceptual framework of 2D-NMR to nonlinear excitations of infrared (vibrational) transitions instead of spin transitions. The nuclear spins are replaced by the amide I vibrational modes (which consist mainly of C=O stretching of the peptide-linkage groups); the RF pulses are replaced by (sub)picosecond IR pulses; the spin–spin couplings by the couplings between the amide I modes, which are, to a large extent, electrostatic, and depend strongly on the distance and orientation of the transition dipoles. The above-mentioned NMR methods can more or less be mapped onto 2D-IR, but with two important differences. First, the timescale of the experiment is less than a picosecond; hence, real-time measurements (e.g. measuring 2D-IR spectra after optically triggering a change in the conformation) can be performed with picosecond time resolution. Second, the frequency splittings between amide I modes are of the order of 10–100 cm^{-1}, so in relaxation (NOE-type) measurements, the spectral density of the fluctuations will be sampled at timescales of 0.1–1 ps.

Another aspect, also related to the different timescale of both techniques, is the capability of 2D-IR spectroscopy to observe conformational sub-states of a peptide. The major degrees of freedom of the polypeptide chain are the (ϕ, ψ) dihedral angles of the two σ-bonds of each amino acid, which can rotate almost freely. A complex balance of forces results in two dominant free energy minima within the (ϕ, ψ) configuration space, corresponding to the two most important secondary structure motifs, α-helices and β-sheets. The almost equal depth of these free energy minima gives rise to the tremendous structural diversity we observe in proteins. However, in the case of small peptides, one expects to obtain a distribution of conformations owing to the shallow free energy potential surface, since intramolecular hydrogen bonds, that stabilize secondary structures, are generally missing in these small systems. Since conformational jumps between conformational sub-states occur many times on the NMR timescale (1–100 ms), NMR techniques probe the time-averaged conformation, which does not necessarily coincide with any of the conformational sub-states. This problem is one reason for a lack of reliable information on the conformation of protein building blocks. The IR timescale (1 ps), on the other hand, is sufficiently fast to freeze conformational states and potentially separate them.

In this paper, we intend to give an overview of the potential of 2D-IR spectroscopy to study conformation and conformational dynamics of small peptides in solution, focusing mainly on our recent work in this direction. The paper is organized as follows. First (section 2), the principles of the method are discussed: in particular, how the couplings between amide I modes can be determined, and how these couplings are quantitatively related to the secondary peptide structure. We end this section with a comparison between the different experimental implementations of 2D-IR spectroscopy (time and frequency domain), showing their equivalence. We then demonstrate how the conformation of a small peptide can be derived from its 2D-IR spectrum (section 3.1), and how time-resolved 2D-IR spectroscopy can be used to investigate conformational fluctuations (sections 3.2 and 3.3). We conclude with a comparison between 2D-IR and other vibrational spectroscopic methods (section 4) and a discussion of future prospects (section 5).

2. Principle of 2D-IR spectroscopy of peptides

To demonstrate the principle of 2D-IR spectroscopy, we show in figure 1 the 2D-IR spectrum of a model system of two coupled vibrators, together with the linear (1D) IR spectrum (above and on the left). For each resonance of the system, a signal consisting of a negative (depicted in blue) and a positive (depicted in red) peak appears along the diagonal of the 2D-IR spectrum.

The structure-related information is in the off-diagonal signals, which also consist of a positive and a negative peak. Exactly as in 2D-NMR spectroscopy [9], these cross peaks appear only when the corresponding resonances at the diagonal are coupled, and from the amplitude of the cross peaks the strength of the coupling can be deduced. Since the coupling strengths are determined by the geometry of the peptide chain, 2D-IR spectroscopy can be used to determine the backbone conformation of small peptides in a similar way to 2D-NMR.

In the remainder of this section, we will first discuss the Hamiltonian used to describe the 2D-IR response, and we will show that 2D-IR spectroscopy directly measures the couplings between the amide I modes in a peptide (section 2.1). A very important property of 2D-IR spectroscopy is the intuitive picture it may provide in directly connecting the spectrum to certain elements of the coupling Hamiltonian (see figure 1). In certain limits, this remains true even when considering the time dependence of the coupling Hamiltonian caused by fluctuations of the surrounding solvent and the molecule itself (section 2.2).

2.1. The static coupling Hamiltonian

The model Hamiltonian used to calculate figure 1 is based on the picture of vibrational excitonic states (vibrons) to describe the nonlinear response of the amide I band. This model separates off the amide I manifold of states from all other vibrational degrees of freedom of the molecule [37–39] and describes the coupling between various amide I modes using the Frenkel-exciton Hamiltonian [40]:

$$H = \sum_i \epsilon_i b_i^\dagger b_i + \sum_{i<j} \beta_{ij}(b_i^\dagger b_j + b_j^\dagger b_i). \tag{1}$$

Here, $b_i^\dagger$ and b_i are the creation and annihilation operators of individual peptide units (sites), respectively, which in the harmonic case would obey the commutation relations

$$\begin{aligned} [b_i^\dagger, b_j] &= \delta_{ij} \\ [b_i^\dagger, b_j^\dagger] &= 0. \end{aligned} \tag{2}$$

The ϵ_i are the intrinsic excitation energies of the individual sites, and the β_{ij} are the couplings between sites. Owing to its simple and physically very intuitive picture, the exciton model is now commonly used to interpret 2D-IR experiments [15–33].

The traditional, and by far more common, picture, however, to describe molecular vibrations is that of normal modes [41, 42]. It had initially been used by Tokmakoff and co-workers to interpret 2D-IR experiments on a metal–carbonyl compound [34–36]. The exciton picture and the normal-mode picture are identical (in certain limits), and merely use different languages. Below, we shall review the connection between the two points of view. In both cases, we describe the amide I band as *coupled, weakly anharmonic oscillators*. The coupling is assumed to be *bilinear* (linear in the displacements of each of the two coupled modes).

We start by noting that the anharmonicity of the amide I band is a weak effect: the difference Δ between the $v = 0 \rightarrow 1$ absorption frequency and the $1 \rightarrow 2$ absorption frequency of the amide I mode is 16 cm^{-1} [15], and Δ/ω is only 1%. Nevertheless, since the nonlinear response of a harmonic system vanishes exactly [43], the anharmonicity is an essential condition for nonlinear vibrational spectroscopy (including 2D-IR) to be possible. It may be pointed out that the two-level systems which are studied in 2D-NMR [9] and 2D-optical spectroscopy [44–47] could be considered as systems with infinite anharmonicity (with the '$v = 2$' state at infinite energy). An elegant way to continuously switch between both limits has been given by Mukamel and co-workers using nonlinear exciton equations [28].

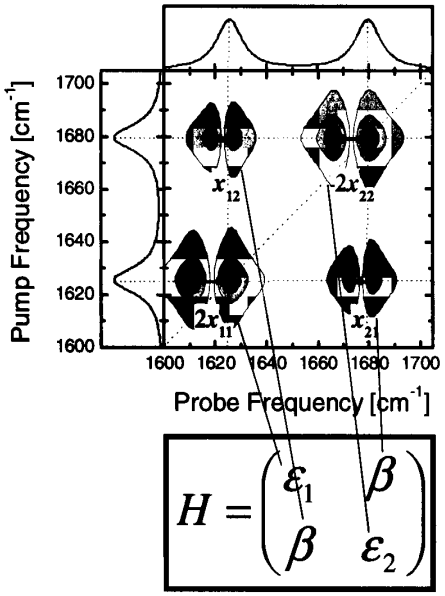

Figure 1. Calculated 2D-IR spectrum of a system consisting of two coupled oscillators. Negative signals (bleach and stimulated emission) are depicted in blue, while positive signals (excited state absorption) are depicted in red. The linear IR spectrum is plotted above and on the left of the 2D plot. The relation between the signals and the corresponding elements of the coupling Hamiltonian equation (5) is depicted.

To illustrate the difference between coupled harmonic and anharmonic oscillators, we discuss them separately.

2.1.1. Coupled harmonic oscillators. A system of coupled harmonic oscillators is described by the Hamiltonian (1). It conserves the number of excitations and hence separates into blocks of the ground state, the one-excitonic Hamiltonian $H_1^{(0)}$, the two-excitonic Hamiltonian $H_2^{(0)}$, etc. When ordering the site basis of a system of two peptide units as

$$\{|0',0'\rangle, |1',0'\rangle, |0',1'\rangle, |2',0'\rangle, |0',2'\rangle, |1',1'\rangle\}, \tag{3}$$

where $|m',n'\rangle$ denotes the state in which the peptide units have m and n vibrational quanta, respectively, and the prime denotes site-basis states, the harmonic Hamiltonian is

$$H^{(0)} = \left(\begin{array}{c|cc|ccc} 0 & & & & & \\ \hline & \epsilon_1 & \beta_{12} & & & \\ & \beta_{12} & \epsilon_2 & & & \\ \hline & & & 2\epsilon_1 & 0 & \sqrt{2}\beta_{12} \\ & & & 0 & 2\epsilon_2 & \sqrt{2}\beta_{12} \\ & & & \sqrt{2}\beta_{12} & \sqrt{2}\beta_{12} & \epsilon_1+\epsilon_2 \end{array}\right). \tag{4}$$

Here, the zero-, one- and two-exciton manifolds have been separated by lines. In the harmonic case, we know without explicit diagonalization of the harmonic two-excitonic

Hamiltonian that its eigenstates (i.e. the two-excitonic states) are product states of the one-excitonic states. In that sense, the one-exciton Hamiltonian:

$$H_1^{(0)} = \begin{pmatrix} \epsilon_1 & \beta_{12} \\ \beta_{12} & \epsilon_2 \end{pmatrix} \tag{5}$$

already contains all the physics of a harmonic system.

In the more traditional normal-mode picture, one would describe the nuclear potential energy surface as a function of nuclear coordinates q_1 and q_2 (in the present case the amide I displacements, which are assumed to be localized on the corresponding sites):

$$V^{(0)}(q_1, q_2) = \tfrac{1}{2}\epsilon_1 q_1^2 + \tfrac{1}{2}\epsilon_2 q_2^2 + \beta_{12} q_1 q_2 \tag{6}$$

with the bilinear coupling term $\beta_{12}q_1q_2$. Diagonalization leads to delocalized normal modes. Equations (1), (4) and (6) all describe the same physical situation, albeit in different languages.

2.1.2. Coupled anharmonic oscillators. As mentioned earlier, we have to include anharmonicity in order to understand the nonlinear spectroscopic response of a system of coupled oscillators. Anharmonicity is generally included in an *ad hoc* manner [15] by lowering the site energies of the doubly excited site states by an energy Δ (see figure 2(b)):

$$H = \left(\begin{array}{c|cc|ccc} 0 & & & & & \\ \hline & \epsilon_1 & \beta_{12} & & & \\ & \beta_{12} & \epsilon_2 & & & \\ \hline & & & 2\epsilon_1 - \Delta & 0 & \sqrt{2}\beta_{12} \\ & & & 0 & 2\epsilon_2 - \Delta & \sqrt{2}\beta_{12} \\ & & & \sqrt{2}\beta_{12} & \sqrt{2}\beta_{12} & \epsilon_1 + \epsilon_2 \end{array}\right). \tag{7}$$

The magnitude of the site anharmonicity $\Delta = 16\,\mathrm{cm}^{-1}$ has been determined from pump–probe experiments on the amide I band of an isolated peptide unit (*N*-methyl acetamide) [15]. In the weak-coupling limit $\beta_{12} \ll |\epsilon_2 - \epsilon_1|$, the two-excitonic states can still be identified as product states of the one-excitonic states, lowered by diagonal and off-diagonal anharmonicity. The latter can be calculated perturbatively [16, 18]:

$$x_{12} = 4\Delta \frac{\beta_{12}^2}{(\epsilon_2 - \epsilon_1)^2}. \tag{8}$$

This approach is equivalent to using a nuclear potential energy surface which includes higher powers of the nuclear coordinates:

$$V(q_1, q_2) = \tfrac{1}{2}\epsilon_1 q_1^2 + \tfrac{1}{2}\epsilon_2 q_2^2 + +\beta_{12} q_1 q_2 + \tfrac{1}{6}\chi_{111} q_1^3 + \tfrac{1}{2}\chi_{222} q_2^3 + \cdots. \tag{9}$$

It is important to note that the anharmonic terms $\frac{1}{6}\chi_{iii}q_i^3$ are assumed to be localized on individual sites, whereas terms such as $\frac{1}{6}\chi_{iij}q_i^2 q_j$ with $i \neq j$ are neglected. This assumption simply expresses that the C=O bond is a dissociative bond which is better described by a Morse potential rather than by a harmonic potential. However, since the leading *linear* coupling term β_{ij} is already weak, we can safely neglect mixed anharmonic coupling terms such as $\chi_{iij}q_i^2 q_j$ with $i \neq j$.

When the normal modes of the potential energy surface equation (9) are calculated by diagonalization of the harmonic part $V^{(0)}(q_1, q_2)$ (equation (6)), the cubic (and higher-order) terms lead to diagonal and off-diagonal anharmonicity x_{ii} and x_{ij}, respectively. In this picture, the vibrational energy of a molecule is expanded in powers of the excitation level n_i of each normal mode [41, 42]:

$$E = \sum_i \epsilon_i (n_i + \tfrac{1}{2}) - \sum_{i \leqslant j} x_{ij}(n_i + \tfrac{1}{2})(n_j + \tfrac{1}{2}) + \cdots. \tag{10}$$

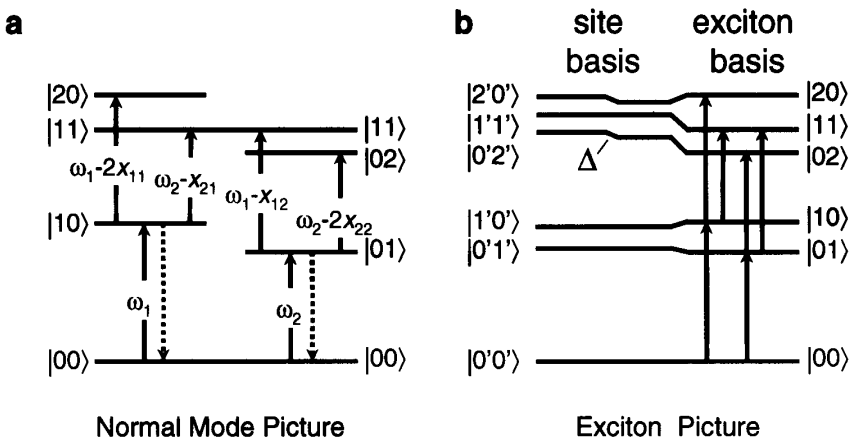

Figure 2. Level scheme of a system of two normal modes $|1, 0\rangle$ and $|0, 1\rangle$ in the normal mode picture (a) and in the exciton picture (b). The double excited state, called overtones $|2, 0\rangle$ and $|0, 2\rangle$ and the combination mode $|1, 1\rangle$ in the normal mode picture (a) or the two-excitonic states in the exciton picture (b), are lowered by the anharmonic constants x_{ij} from the value one would obtain in the harmonic limit. The arrows depict the harmonically allowed transitions with a colour coding that is the same as in figure 1.

Perturbative equations to express the anharmonic constants x_{ii} and x_{ij} in terms of a cubic and quartic expansion of the nuclear potential surface have been worked out, e.g. in [48–51]. It is easily seen that $x_{ij} = 0$ when $\beta_{ij} = 0$ (assuming $\chi_{iij} = 0$ for all $i \neq j$). Furthermore, one can show in a straightforward manner that the diagonal and off-diagonal anharmonicities obtained from equation (9) are equal to the perturbative solution equation (8).

Figure 2 shows a level scheme for a system of two vibrational modes $|1, 0\rangle$ and $|0, 1\rangle$ in two complementary representations, chosen to illustrate both points of view: (a) the normal mode picture adapted from [34] and (b) the exciton picture adapted from [15]. The doubly excited states are called overtones ($|2, 0\rangle$ and $|0, 2\rangle$) and combination mode ($|1, 1\rangle$) in the normal mode picture, and two-exciton states in the excitonic picture, respectively. Their energies are lowered by the anharmonic constants x_{ij} from the value one would find in the harmonic limit. The level scheme emphasizes that the shift between the negative bleach signal (depicted in blue in figure 1) and the positive excited state absorption signal (depicted in red in figure 1) directly represents the anharmonic constants x_{ij}. Consider, for example, a pump frequency resonant with the absorption line at ω_1. In that case, the state $|1, 0\rangle$ will be populated and the common ground state $|0, 0\rangle$ will be depleted. Consequently, a decrease in absorption (negative signal) will be observed not only at frequency ω_1, but also at frequency ω_2 (corresponding to the transition $|0, 0\rangle \rightarrow |0, 1\rangle$). In addition, an excited-state absorption signal will emerge with frequency $\omega_2 - x_{21}$, corresponding to the transition $|1, 0\rangle \rightarrow |1, 1\rangle$. The two signals together result in the lower-right cross peak in figure 1. When the coupling β_{12} vanishes, the off-diagonal anharmonicity x_{12} also vanishes. In that case, both signals contributing to the cross peak appear at the same frequency and cancel exactly. *Hence, the intensity of the cross peak is a direct measure of the coupling β between two peptide units* (see figure 1).

To summarize this paragraph, one would in principle need to know all the mixed cubic and quartic derivatives of the molecular potential surface in order to exactly calculate the

diagonal and off-diagonal anharmonicities [49–51], and hence the 2D-IR response. This is an unfeasible task for a molecule as large as a peptide [52]. Nevertheless, the simplifying assumption concerning the nuclear potential surface equation (9), namely the assumption of only bilinear coupling and $\chi_{iij} = 0$ for $i \neq j$, allows one to use the exciton model as a much simpler approach. The anharmonic one-exciton Hamiltonian is the same as in the harmonic case (equation (5)), and the only additional parameter is the diagonal anharmonicity Δ, which enters only into the two-exciton Hamiltonian. As it reflects a property of the individual peptide units, one can safely assume that this parameter is a constant which does not depend on the geometry of the peptide backbone. In other words, the one-exciton Hamiltonian (5) describes all the physics of the coupling between different amide I states, which is directly related to the geometry of the molecule (see the next subsection). Only one additional parameter (Δ) enters to describe the anharmonicity of the system, which is needed to relate the excitonic coupling scheme to nonlinear IR spectroscopy. This renders the exciton coupling model a simple and powerful way of describing 2D-IR spectroscopy of (poly)peptides.

It is instructive to discuss this point from yet another perspective. As long as only the harmonic Hamiltonian equation (4) is considered, the coupling β_{12}, defined in the site basis, appears to be artificial since if one were to transform the Hamiltonian equation (4) into a normal mode basis by diagonalizing it, any coupling would vanish. In other words, the coupling β_{12} appears to be the result of a wrong choice of the basis set. Hence, the question arises as to which property distinguishes the site basis. The answer is the localized anharmonicity described by terms $\frac{1}{6}\chi_{iii}q_i^3$ in equation (9), which expresses that the C=O bond is dissociative. While we can understand coupling already in the harmonic limit, the anharmonicity is required for an observable signal in the nonlinear third-order spectroscopic experiment, from which the magnitude of the coupling can be derived. However, anharmonicity does not add any complexity to the problem, since all physics of the system is already contained in the one-exciton Hamiltonian equation (5).

2.1.3. Coupling models. Up to this point, we have discussed the principle of 2D-IR spectroscopy without specifying the origin of the coupling β_{ij}. In all practical applications, 2D-IR spectroscopy relies on the fact that the coupling between adjacent amide I modes is in some way related to the geometry of the molecule. The simplest and very intuitive approach to relate the coupling constant to the peptide geometry is the transition dipole coupling (TDC) model introduced by Krimm *et al* [53] and Torii *et al* [37], which is based on two crude approximations: (a) the dipole approximation and (b) neglect of through-bond effects. It is well established that the amide I vibration (which is mostly the C=O stretching vibration) is accompanied by a charge flow between the carbonyl oxygen and the nitrogen, which is responsible for about 1/2 of the total transition dipole moment of the amide I mode [53]. Hence, the size of the object (2.5 Å) which gives rise to the transition dipole is of the same order as the distance between adjacent amide I groups. As a consequence, it is extremely questionable whether the dipole approximation can be used. Furthermore, normal mode calculations on *N*-methylacetamide (NMA, CH_3–CONH–CH_3) show that the amide I vibration is not entirely localized on the peptide unit (–CO–NH–) and that methyl carbon and hydrogen atoms are involved as well [16]. Hence, through-bond effects will certainly contribute to the coupling between chemically bonded peptide units.

The most sophisticated way of calculating couplings between amide I modes would be from *ab initio* normal mode calculations of the complete polypeptide. With the present computer power, this is feasible only for extremely small peptides, such as di- and tripeptides, but becomes impossible for larger polypeptides. Moreover, a structure determination will require some sort of optimization algorithm, which iteratively varies the conformation of a

test molecule, calculates a set of coupling constants for each configuration and compares them with the experimental data. Since this will be a high-dimensional optimization problem (except for the smallest peptides) it will require many calculations of coupling constants, and it is necessary to seek for the least computer-expensive, but still sufficiently accurate, methods to calculate a set of coupling constants for a given conformation. We have recently compared several approaches to calculate vibrational coupling constants: TDC, transition charge coupling, molecular orbital calculations and *ab initio* normal mode calculations [54]. These methods are increasingly sophisticated and (hopefully) accurate, but also increasingly computer-expensive. It turns out that the dipole approximation is too crude to be useful when aiming for quantitative results. The accuracy of higher level methods depends on the conformational region under study. As long as only a two-dimensional (ϕ, ψ) conformational space is to be explored, it is still feasible to assemble a map using *ab initio* normal mode calculations (about 1 CPU-day for each point with present computer power), which takes into account all through-space and through-bond effects. Such a map can easily be parametrized. However, for a larger than two-dimensional configurational space, i.e. for larger peptides, this approach becomes impossible. Hence, a mixed strategy is proposed: nearest-neighbour coupling, for which through-bond effects are essential, should be calculated on the highest available level, using a pre-parametrized map. For peptide units that come close in space, but that are not adjacent in the polypeptide chain, through-bond effects are certainly much less important and cheaper methods, such as the approach using transition charges, can be used.

2.2. *The time-dependent coupling Hamiltonian*

In solution, the molecule will be in a fluctuating environment, and the coupling Hamiltonian equation (1) will be time dependent:

$$H(t) = \begin{pmatrix} \epsilon_1(t) & \beta_{12}(t) \\ \beta_{12}(t) & \epsilon_2(t) \end{pmatrix} \equiv \begin{pmatrix} \epsilon_1 + \delta\epsilon_1(t) & \beta_{12} + \delta\beta_{12}(t) \\ \beta_{12} + \delta\beta_{12}(t) & \epsilon_2 + \delta\epsilon_2(t) \end{pmatrix} \tag{11}$$

where $\delta\epsilon_1(t)$, $\delta\epsilon_2(t)$ and $\delta\beta_{12}(t)$ are the instantaneous deviations of the site energies and couplings from their time-average values ϵ_1, ϵ_2 and β_{12} with vanishing time average $\langle\delta\epsilon_1(t)\rangle = 0$, $\langle\delta\epsilon_2(t)\rangle = 0$ and $\langle\delta\beta_{12}(t)\rangle = 0$. While evaluation of this expression becomes quite involved in the general case [29], it still decouples into simple and very intuitive terms in the weak coupling limit $\beta_{12} \ll |\epsilon_2 - \epsilon_1|$. To this end, we diagonalize the Hamiltonian equation (11) with respect to its time average part up to first order of the mixing angle (the smallness parameter):

$$\phi \approx \frac{\beta_{12}}{\epsilon_2 - \epsilon_1} \tag{12}$$

and obtain

$$H'(t) = H_{\text{stat}} + H^{(0)}_{\text{dyn}}(t) + H^{(1)}_{\text{dyn}}(t) + \cdots \tag{13}$$

with

$$\begin{aligned} H_{\text{stat}} &= \begin{pmatrix} \epsilon_1 - 2\phi \cdot \beta_{12} & 0 \\ 0 & \epsilon_2 + 2\phi \cdot \beta_{12} \end{pmatrix} \\ H^{(0)}_{\text{dyn}}(t) &= \begin{pmatrix} \delta\epsilon_1(t) & \delta\beta_{12}(t) \\ \delta\beta_{12}(t) & \delta\epsilon_2(t) \end{pmatrix} \\ H^{(1)}_{\text{dyn}}(t) &= \begin{pmatrix} -2\phi \cdot \delta\beta_{12}(t) & \phi \cdot \delta\Delta\epsilon(t) \\ \phi \cdot \delta\Delta\epsilon(t) & 2\phi \cdot \delta\beta_{12}(t) \end{pmatrix} \end{aligned} \tag{14}$$

and $\delta\Delta\epsilon(t) = \delta\epsilon_1(t) - \delta\epsilon_2(t)$. The first term H_{stat} is the static contribution which is diagonal by construction, the second term $H^{(0)}_{\text{dyn}}(t)$ is zero order in the mixing angle ϕ and the third term

is $H^{(1)}_{\rm dyn}(t)$ first order in the mixing angle ϕ. The time averages $\langle H^{(0)}_{\rm dyn}(t)\rangle = 0$ and $\langle H^{(1)}_{\rm dyn}(t)\rangle = 0$ vanish.

To zeroth order of $\phi = \beta_{12}/(\epsilon_2 - \epsilon_1)$, the time dependence of the coupling Hamiltonian separates completely, leading to the simple picture sketched in figure 1. The time dependence of the diagonal peaks (dephasing and spectral diffusion) is governed solely by fluctuations of the diagonal elements $\delta\epsilon_1(t)$ and $\delta\epsilon_1(t)$, while the time dependence of the cross peaks (cross relaxation) is exclusively governed by fluctuations of the off-diagonal elements $\delta\beta_{12}(t)$. This is the level of theory which is generally sufficient in NMR spectroscopy [8]. It is not immediately obvious that it is also sufficient in the case of vibrational transitions, since typically the mixing angles are larger. However, it has been verified using MD simulations [22, 23] that the first-order term $H^{(1)}_{\rm dyn}(t)$ contributes only little in the example considered in section 3. When higher-order terms become important, fluctuations of diagonal terms start to contribute to the time dependence of the cross peaks and *vice versa* through the term $H^{(1)}_{\rm dyn}(t)$.

2.2.1. Dephasing and spectral diffusion. Within the zeroth-order approximation described above, the lineshape function of each diagonal peak in the 2D spectrum can be treated as if it were a separated (uncoupled) state. To this end, we use the Kubo picture of stochastic fluctuations of the transition frequency as a result of perturbations by a fluctuating surrounding (which can be inter- or intramolecular degrees of freedom) [55]. In this approach, both linear and nonlinear spectroscopy are described in terms of the *frequency fluctuation autocorrelation function* $\langle\delta\epsilon_i(t)\delta\epsilon_i(0)\rangle$ $(i = 1, 2)$. Employing time-dependent perturbation theory, the linear absorption spectrum can then be written as

$$I(\omega) = \mathrm{Re}\int_0^\infty \mathrm{d}t\, \mathrm{e}^{-\mathrm{i}(\omega-\epsilon/\hbar)t}\mathrm{e}^{-g(t)-t/2T_1}, \tag{15}$$

where the $v = 0 \rightarrow 1$ transition is determined by the lineshape function

$$g(t) = \int_0^t \mathrm{d}\tau' \int_0^{\tau'} \mathrm{d}\tau''\, \langle\delta\epsilon_i(\tau'')\delta\epsilon_i(0)\rangle, \tag{16}$$

as well as by the vibrational energy relaxation time T_1. Within the limits of the second-order cumulant expansion, the formulation is readily extended to calculate the third-order nonlinear response functions $R(t_1, t_2, t_3)$ [18, 43, 56], which yield the 2D lineshape after convolution with the pulse envelopes [23, 45, 47, 57, 58]:

$$P^{(3)}(t) = \int_0^\infty \mathrm{d}t_3 \int_0^\infty \mathrm{d}t_2 \int_0^\infty \mathrm{d}t_1\, R(t_1, t_2, t_3)E_3(t - t_3)E_2(t - t_3 - t_2)E_1^*(t - t_3 - t_2 - t_1) \tag{17}$$

where E_1, E_2 and E_3 are the incident laser fields for the particular experimental configuration chosen (see section 2.3).

One commonly finds that the frequency fluctuation correlation function decays on (at least) two timescales [59]: (i) An ultrafast, inertial component on a 50–100 fs timescale and (ii) a slower, diffusion-controlled component. In the case of vibrational transitions, the ultrafast component is typically in the motional narrowing limit, i.e. its correlation time τ_c is much faster than the effective dephasing time T_2^* [18, 56]. In that limit, its timescale is not directly observable since it is hidden underneath the homogeneous linewidth of the transition (note that this an intrinsic limitation and is not due to the time resolution of the laser system). Only the pure dephasing time can be determined, which is calculated as $T_2^* = \langle\Delta^2\rangle \cdot \tau_c$, where Δ is the amplitude of the fast component. The slower process, however, is directly observable as a change of the tilt of the 2D line with increasing mixing time τ_m (see section 3.3) [23, 45, 47, 57, 58].

2.2.2. Cross relaxation. In zeroth order of the mixing angle $\phi = \beta_{12}/\Delta\epsilon$, fluctuation of off-diagonal elements $\delta\beta_{12}$ lead to irreversible cross relaxation of population between the two eigenstates of Hamiltonian H_{stat} (equation 14) with increasing mixing time τ_m. Its rate is determined by Fermi's golden rule [8]:

$$k = \frac{1}{\hbar^2}\int_{-\infty}^{\infty}\langle\delta\beta_{12}(t)\delta\beta_{12}(0)\rangle e^{i\Delta\epsilon\, t/\hbar}\,dt \tag{18}$$

which depends solely on fluctuations of the coupling $\delta\beta_{12}(t)$. When the first-order term $H^{(1)}_{\text{dyn}}(t)$ becomes important, the correlation function $\langle\delta\Delta\epsilon(t)\delta\Delta\epsilon(0)\rangle$ and the cross-correlation function $\langle\delta\beta_{12}(t)\delta\Delta\epsilon(0)\rangle$ may also contribute to cross relaxation [22].

2.3. Experimental methods

A variety of 2D vibrational spectroscopies have been proposed theoretically [33, 60–62] and implemented experimentally [63–68]. Many of these techniques are based on Raman transitions and utilize ultrashort optical pulses for impulsive excitation, where at least one field interaction induces a two-quantum transition. This explains why the nonlinear response of these techniques is inherently very weak, and why these experiments are extremely challenging. Here, we concentrate on 2D vibrational spectroscopies utilizing resonant, semi-impulsive excitation with infrared pulses [15–36], which implies that all transitions involved are one-quantum transitions (see figure 2). The same concept has also been applied to electronic transitions by the Jonas group [44–47].

Two experimental techniques have been utilized to measure such 2D-IR spectra: *double-resonance* or *dynamic hole burning* experiments [15, 16, 19–24] and *pulsed Fourier transform* or *heterodyne detected photon echo* experiments [25–27, 34–36]. The former is a quasi-frequency domain technique (quasi-frequency domain technique in the sense that the pump pulse is spectrally selective, but still relatively short, and offers significant time resolution), while the latter is a pure time-domain technique. The two techniques are complementary [69] and provide specific advantages and disadvantages, which shall be discussed in the following. Figures 3(a) and (b) shows the principle of the set-ups of both techniques and the pulse sequence in the sample.

2.3.1. Double-resonance experiment. The double-resonance experiment is essentially a conventional pump–probe experiment. One starts from an intense, ultrashort (typically 100 fs) IR laser pulse [70], the bandwidth of which ($\approx$200 cm^{-1}) covers the whole spectral range of interest. The pulse is split into pump and probe beam, one of which passes a computer controlled delay line (i.e. the mixing time τ_m), and both are spatially recombined in the sample. The probe beam is subsequently frequency dispersed in a spectrometer and detected in an IR array detector. What differentiates the double-resonance experiment from a conventional pump–probe experiment is the adjustable Fabry–Perot filter which the pump beam passes before hitting the sample. It consist of two partial reflectors separated by a distance which is regulated by a feedback-controlled piezoelectric mount, and slices out narrow-band pump pulses (bandwidth 11 cm^{-1}, FWHM $\sim$750 fs), the centre frequency of which can be varied by adjusting the Fabry–Perot filter. In this way, two frequency axes are defined, the centre frequency of the pump pulse and the probe frequency. These are the frequency axes used in the 2D representation of figure 1. In other words, the two-dimensional (2D) plots are stacks of transient spectra, each horizontal cross section representing a transient absorption spectrum obtained by pumping at the frequency on the vertical axis. In the 2D spectra one observes the bleach and stimulated emission of the $v = 0 \rightarrow 1$ amide I transition as the negative

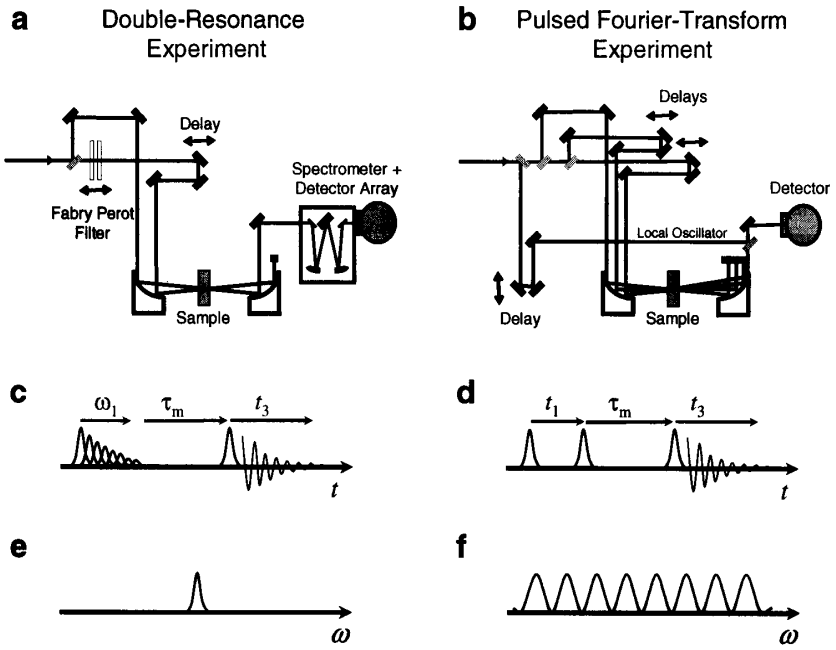

Figure 3. Set-up for (a) a double-resonance experiment and (b) a pulsed Fourier transform experiment. Pulse sequence used in both experiments in (c + d) *time domain* and in (e + f) *frequency domain*.

(blue) signal and the $v = 1 \rightarrow 2$ excited-state absorption as the positive (red) signal, the latter occurring at a lower frequency because of the anharmonicity of the amide I mode. As discussed above, the level scheme, figure 2, gives an intuitive explanation for the appearance of the double-resonance 2D-IR spectrum.

2.3.2. Pulsed Fourier transform experiments. The pulsed Fourier transform experiment (or heterodyne-detected photon echo experiment) starts from a conventional three-pulse photon echo experiment [56, 59, 71–76], in which three pulses are directed onto the sample with the delay times between the pulses varied by computer-controlled delay lines. One typically uses the so-called box CARS configuration [77], which allows one to separate the phase matching directions of all ingoing (k_1, k_2 and k_3) and outgoing ($-k_1 + k_2 + k_3$ and $+k_1 - k_2 + k_3$) beams. In a next step, the generated third-order field is 2D-Fourier transformed with respect to times t_1 and t_3 (see figure 3(d)), generating a 2D-IR spectrum as a function of two frequencies ω_1 and ω_3 [25–27, 34–36]. In order to be able to do so, one needs to know the third-order electric field, rather than the time-integrated intensity, which is what 'normal' optical detectors measure. The field is obtained by interferometric superposition of the generated third-order field and a so-called local oscillator field (heterodyning), for which a fourth replica of the initial ultrashort laser pulse is used. The delay times t_1 between the first and second field interaction and t_3 between the generated third-order field and the local oscillator have to be

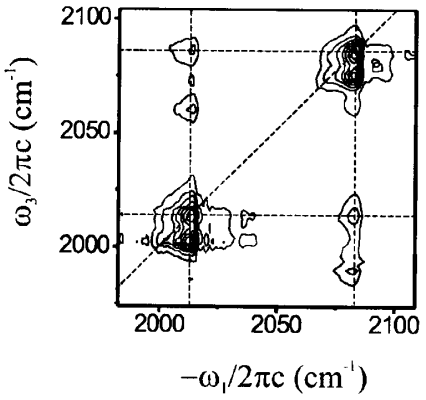

Figure 4. Pulsed Fourier transform 2D-IR spectrum of the symmetric and asymmetric C + O stretch vibrations of dicarbonylacetylacetonato rhodium (I) (RDC) dissolved in hexane. Adapted from [34].

phase-stabilized. Fortunately, the large wavelength of the IR light gives rise to the hope that one can rely on the mechanical stability of the set-up without active stabilization of the field phases. A promising approach to significantly improve phase stability, based on diffractive optics, has been proposed and implemented by Miller and co-workers [78, 79]

Despite the apparent differences in the measuring techniques, the resulting 2D-IR spectra are remarkably similar. This is seen, for example, when comparing figure 1, calculated for the double-resonance experiment, and figure 4, which is a pulsed Fourier transform 2D-IR spectrum of the symmetric and asymmetric C=O stretch vibrations of dicarbonylacetylacetonato rhodium (I) (RDC) dissolved in hexane (adapted from [34] and kindly provided to us by Andrei Tokmakoff). This system has sufficiently narrow absorption bands that all transitions in the 2D spectrum are separately observable. As in figure 1, the separation between both contributions to each diagonal and off-diagonal peak directly represents diagonal and off-diagonal anharmonicities $2x_{ii}$ and x_{ij}, respectively, which are well known for this molecule (note that the x and y axes are interchanged in figures 1 and 4). In fact, Tokmakoff and co-workers have used the double-resonance picture, to discuss a pulsed Fourier transform 2D-IR spectrum [34–36].

The similarity between the two types of experiment is no coincidence. Both experiments probe the same third-order response function $R(t_1, t_2, t_3)$, which is the property that describes the system, and differ only in the way the laser fields E_1, E_2, and E_3 read out that response function through equation (17) (see, e.g., [18, 43]). In fact, the quasi-frequency-domain experiment (i.e. the double-resonance experiment) and the time-domain experiment (i.e. the heterodyned photon echo experiment) are connected by straightforward Fourier transformation. In simple words, in the first case the Fourier transformation is performed by the Fabry–Perot filter and the spectrometer, whereas in the second case it is performed numerically in the computer. In fact, the Fourier transformation with respect to time t_3 has also been performed in a spectrometer in pulsed Fourier transform experiments [34–36, 44, 45, 80]. The only difference between both experimental techniques therefore relates to time t_1 and the first two field interactions.

Figures 3(c) and (d) compare the pulse sequences in the sample generated by both techniques in the *time domain*. The pulsed Fourier transform experiment uses two separate pulses for the first two field interactions. Both the delay time and relative phase between

these two pulses have to be controlled in the experiment. In contrast, the double-resonance experiment uses a multiple pulse sequence for the first two field interactions, namely the output of the Fabry–Perot filter. The sequence of pulses replaces the scanning of the delay time between the first two field interactions. The relative phase of the pulses in the sequence, on the other hand, is controlled by fine-tuning the distance between the Fabry–Perot mirrors.

In the *frequency domain*, the multiple sequence of pulses in the double-resonance experiment corresponds to a relatively narrow pump pulse which selectively excites individual transitions (figure 3(e)). Spectral interference of the first pair of pulses in the pulsed Fourier transform experiment, on the other hand, corresponds to an excitation spectrum which has a sinusoidal shape, with a period determined by the time delay between the two pulses (figure 3(f)), and which possibly excites more than one transition (depending on the period of the sinusoidal spectrum). Since the subsequent probe process by the third field interaction, which is identical in both approaches, is linear in the non-equilibrium density matrix generated by the first two field interactions, the sinusoidal excitation spectrum will generate a *linear* superposition of signals. This is why it makes no difference whether one performs the Fourier transform with respect to time t_1 before interaction with the sample, i.e. in the Fabry–Perot filter, or afterwards in the computer.

It should, however, be noted that there are indeed conceptual differences between both types of experiments, which are based on the fact that one has independent control over the parameters of all three field interactions in the three-pulse photon echo experiment, while the first two field interactions in the double-resonance experiment originate from one laser beam with necessarily the same parameters. This advantage has recently been demonstrated very elegantly by Hochstrasser and co-workers, who showed that, by independent control of the polarization of all three laser beams, one can directly suppress the often dominating diagonal contribution in a 2D-IR spectrum [27] (see section 3.1).

Furthermore, the three-pulse photon echo experiment allows one to discriminate between different Liouville pathways, namely those emitting in the $-k_1 + k_2 + k_3$ and $+k_1 - k_2 + k_3$ directions [43]. Since the first two field interactions in the double-resonance experiment originate from one laser pulse, both time orderings $-k_1 + k_2 + k_3$ and $+k_1 - k_2 + k_3$ occur simultaneously. Interestingly, it has been argued that the direct analogue to 2D-NOESY spectroscopy in NMR [9] should use a sum of both time orderings [31, 46], which is already implicitly done in the double-resonance experiment.

To conclude this section, the pulsed Fourier transform experiment offers conceptual advantages at the expense of a much more complex, and much more sensitive, experimental set-up (see figures 3(a) and (b)). Only two instead of four laser pulses are needed in the double-resonance experiment, with *no* need of phase stabilization. Furthermore, the double-resonance experiment allows one to exclusively measure the response for one particular pump frequency (i.e. a horizontal cut through the 2D spectrum of figure 1), enabling a longer averaging time and hence a better signal-to-noise ratio. We use this advantage in section 3.2, where population transfer between two amide I modes is measured for long mixing times with exceptionally small signals. In a pulsed Fourier transform experiment, on the other hand, such a cut through the 2D spectrum would still require a complete t_1 data set to be measured in order to perform the 2D-Fourier transform.

3. Structure and dynamics of trialanine

We now demonstrate how the conformation and conformational flexibility of a small peptide can be determined from its 2D-IR spectrum [19, 20, 22, 23], based on the concepts outlined in section 2. For the sake of simplicity, we focus on a system with only two amide I modes. We

have chosen trialanine (see figure 5), since vibrational circular dichroism (VCD) studies [81–83] have suggested that this peptide has a stable conformation in aqueous solution. Since trialanine has only two peptide units, the central backbone conformation is characterized by only a single pair of dihedral angles (ϕ, ψ) (see figure 5). These determine the coupling strength β_{12} between the two amide I oscillators and the angle θ between their transition dipole vectors.

In the remainder of this section, we first discuss the structural preference of trialanine as obtained from the time-independent 2D-IR spectrum by evaluating the cross peak intensity and anisotropy (section 3.1). In a second step, the time evolution of the 2D-IR spectrum is investigated by additionally varying the mixing time τ_m. As emphasized in section 2.2, fluctuations of the diagonal and off-diagonal elements of the coupling Hamiltonian lead to separable time dependence of off-diagonal and diagonal peaks in the 2D-IR spectrum. These will be discussed in sections 3.2 and 3.3, respectively.

3.1. Time-averaged structure

Figure 6(a) shows the linear absorption spectrum of deuterated trialanine in D_2O. It shows two amide I bands, centred at approximately 1650 and 1675 cm^{-1} [81]. Figures 6(b) and (c) show the 2D pump–probe signal for parallel and perpendicularly polarized pump and probe pulses, respectively. At the diagonal of the 2D spectrum one observes the bleach and stimulated emission for each of the two amide I bands as the negative (blue) signal, and the excited-state absorption as the positive (red) signal at lower probe frequency. The pump–probe signal is elongated parallel to the diagonal, indicating that the amide I bands are inhomogeneously broadened [45, 58].

At first sight, no cross peak structure can be distinguished in the 2D spectra, mainly because the cross peaks overlap with the very strong and broad diagonal peaks. Overlap between diagonal and cross peaks is a problem intrinsic to 2D vibrational spectroscopy on peptides, and is due to the fact that the difference between the uncoupled amide I frequencies is of the same order as the coupling strength and the linewidth. The overlap can be strongly reduced by increasing the separation between the amide I frequencies using ^{13}C isotope labelling of one of the peptide units. The result is seen in figure 8(b), where the cross peaks are well separated from the diagonal peaks. This figure should be compared to figure 1 (see section 2.1 for the doublet structure of the cross peaks).

Since the intensity of the cross peaks scales quadratically with the frequency splitting (see equation (8)), its value is much more difficult to determine for the isotope-labelled than for the unlabelled molecule. Fortunately, for unlabelled trialanine the cross peaks can also be separated from the strong diagonal signal by exploiting their dependence on the relative polarizations of the pump and probe pulses. The pumped and probed transition dipoles giving rise to the cross-peak signal are, in general, not parallel, which renders the anisotropy of the cross peaks different from that of the diagonal peaks (which is ideally 2/5). Hence, by subtracting the parallel from the perpendicular scan (both scaled to the maximum occurring on their respective diagonals) the diagonal peaks are eliminated, and the cross peaks revealed (figure 6(d)).

A similar but more elegant method to eliminate the strong diagonal peaks has recently been developed by Hochstrasser and co-workers [27]. This method also relies on the fact that the coupled transition dipoles are generally not parallel to eliminate the diagonal peaks, but uses a specific choice of the relative polarizations of the four optical fields involved in the experiment to eliminate the response in case the transition dipoles involved are parallel (see section 2.3).

Deriving the conformation from the 2D-IR spectrum involves two steps: (i) obtaining from the 2D spectrum the coupling strength β_{12} between the amide I modes and the angle θ between their transition dipoles; (ii) deriving the conformation from the values of these parameters. In the ideal case where the cross peaks are well separated from the diagonal signal, β_{12} can be determined from the cross peak intensity (see section 2.1) and θ from the dependence of the cross peak intensity on the angle between the pump and probe polarizations [16]. In practice, however, one least-squares fits calculated 2D spectra to the experimental ones, using starting values of the parameters obtained by inspection of the experimental 2D spectra. To that end, one calculates the 2D spectrum for a given set of parameter values β_{12} and θ by diagonalizing the Hamiltonian (7) and using third-order perturbation theory [43] to obtain the nonlinear infrared response due to optical transitions between the eigenstates. The parameters are then varied using a nonlinear Levenberg–Marquardt algorithm [84] to find the best agreement with the parallel and perpendicular experimental 2D spectra (see figures 6(e)–(h) for the fitted results). In this way, we obtain $\beta_{12} = 6\ \mathrm{cm}^{-1}$ for the coupling strength and $\theta = 106°$ for the angle between the transition dipole vectors.

The values of β_{12} and θ are determined by the secondary peptide structure, and since the peptide (–CO–ND–) group is essentially planar [85], by the two dihedral angles ϕ and ψ only (see figure 5). The functional relation between the coupling β_{12} and (ϕ, ψ) has been discussed in section 2.1. The relation between the angle θ between the two transition dipoles is determined by geometrical considerations only. Note that θ is the angle between the transition dipoles in the site basis, i.e. in the absence of coupling, and we assume an angle of 20° between the C=O axis and the transition dipole [53]. In figure 7, the coupling strength β_{12} (red contours) and the angle θ (blue contours) are plotted as a function of (ϕ, ψ). Using the map of figure 7, the structure of the peptide can be determined directly from the experimentally determined β_{12} and θ, simply by finding the (ϕ, ψ) coordinates of the points where the $\beta_{12} = 6\ \mathrm{cm}^{-1}$ and $\theta = 106°$ contours intersect. There are two regions where this occurs, $(\phi, \psi) \approx (-60°, 140°)$ and $(\phi, \psi) \approx (60°, -140°)$, situated centre-symmetrically in the Ramachandran plot. Because of sterical hindrance by the residual methyl group of l-alanine [85], only a small range of (ϕ, ψ) values, situated mainly in the left half of the plot, is physically realizable. Hence we conclude that the conformation of trialanine is characterized by $(\phi, \psi) = (-60°, 140°)$, indicated by the arrow in figure 7. In this conformation, the two C=O groups form a left-handed structure, in agreement with the sign of the couplet observed in VCD spectroscopy [81].

It is well established that peptide conformations generally occur in two regions of the (ϕ, ψ) conformational space [85]. The first region, around $(\phi, \psi) = (-60°, -50°)$, is typical for the right-handed α-helix and (with slightly different dihedral angles) the π- and 3_{10}-helix. The second region corresponds to secondary structures such as the anti-parallel β-sheet $(-139°, 135°)$, the parallel β-sheet $(-119°, 113°)$, and the poly(Gly)II (P_{II}) structure $(-80°, 150°)$, the latter of which is very close to the structure derived from the 2D-IR spectrum.

We have verified our methodology by investigating different ^{13}C-isotopomers of trialanine (Ala–Ala–Ala, Ala*–Ala–Ala and Ala–Ala*–Ala) [20]. Even though the molecular Hamiltonian, and hence the 2D-IR spectrum, is different in all three cases, the conformation determined for each of the isotopomers is the same. This finding proves that, in spite of its simplicity, the exciton model, which is at the basis of the structure determination, is accurate enough to extract quantitative information.

An independent confirmation of the conformation predicted here has been obtained from a 20 ns molecular dynamic (MD) simulation of trialanine in water [86]. It was found that the trajectory populates three free-energy minima, the lowest of which at $(\phi, \psi) = (-68°, 141°)$ is in very good agreement with the time-averaged conformation $(\phi, \psi) \approx (-60°, 140°)$ obtained

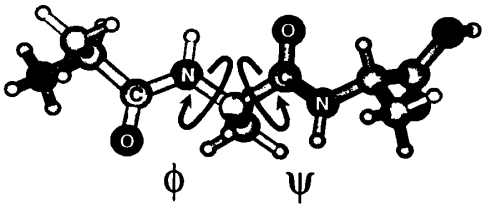

Figure 5. Molecular structure of trialanine. The central dihedral angles (ϕ, ψ) are indicated by arrows.

here. Furthermore, the NMR ^3J-coupling between the C_α and the amide proton [23, 87], which is indicative of the ϕ dihedral angle, supports our structure assignment.

3.2. Conformational flexibility

In solution, the structure of the peptide is not rigid and will fluctuate as a result of perturbations exerted by the solvent molecules on the backbone. As the coupling β_{12} is a function of peptide dihedral angles (ϕ, ψ) [54, 88], a fluctuating backbone translates directly into a stochastic time dependence of the coupling $\beta_{12}(t) = \beta_{12} + \delta\beta_{12}(t)$ between the spectroscopic states of the molecule, leading to irreversible transfer of population (see section 2.2.2). The physical background of this experiment is comparable with that of nuclear Overhauser effect spectroscopy (NOESY) in 2D-NMR spectroscopy, which also measures incoherent population transfer between spin states to investigate conformational fluctuations of peptides and proteins [9, 13]. However, since the typical frequency splittings between amide I states are of the order of 10–100 cm^{-1}, the IR method is specifically sensitive to conformational fluctuations taking place on a 0.1–1 ps timescale.

We have measured 2D spectra of trialanine as a function of the pump–probe delay or 'mixing' time τ_m. Figure 8(a) shows the linear spectrum of Ala–Ala*–Ala, where the asterisk denotes ^{13}C-labelling of the carbonyl carbon atom, and figures 8(b) and (c) show the two-dimensional spectra of Ala–Ala*–Ala at mixing times of 1.5 and 4 ps. The 2D spectrum changes significantly as a function of mixing time, and the relative intensity of the cross peaks increases with increasing mixing time. This is caused by an incoherent population transfer of the vibrational excitation from the optically excited peptide unit to the other peptide unit. For the latter this gives rise to a negative absorption change at the $v = 0 \rightarrow 1$ frequency and a positive absorption change at the $v = 1 \rightarrow 2$ frequency, which is observed in the off-diagonal region of the 2D spectrum. This contribution to the cross peak has essentially the same shape as the coherent cross peak discussed in section 2.1. The two contributions can, however, be clearly distinguished by their mixing-time dependence [9]: the coherent contribution to the cross peak is independent of mixing time, whereas the contribution due to cross relaxation is initially zero and increases with increasing mixing time.

The population ratio of the two amide I modes is obtained by dividing the ratio of the cross and diagonal peaks by an appropriate scaling factor [22]. The ratio of the populations of the two amide I states derived from the data is shown as a function of mixing time in figure 9. Fitting the data yields for the cross relaxation rates 0.07 ± 0.01 and 0.19 ± 0.02 ps^{-1} for Ala–Ala*–Ala and Ala–Ala–Ala, respectively.

The cross relaxation rates are given by the Fourier transform of the coupling autocorrelation function $\langle \delta\beta_{12}(t)\delta\beta_{12}(0)\rangle$, evaluated at the frequency of the energy gap between both states (equation (18)). Assuming that the $\beta_{12}(t)$ fluctuations can be described as a Markovian process,

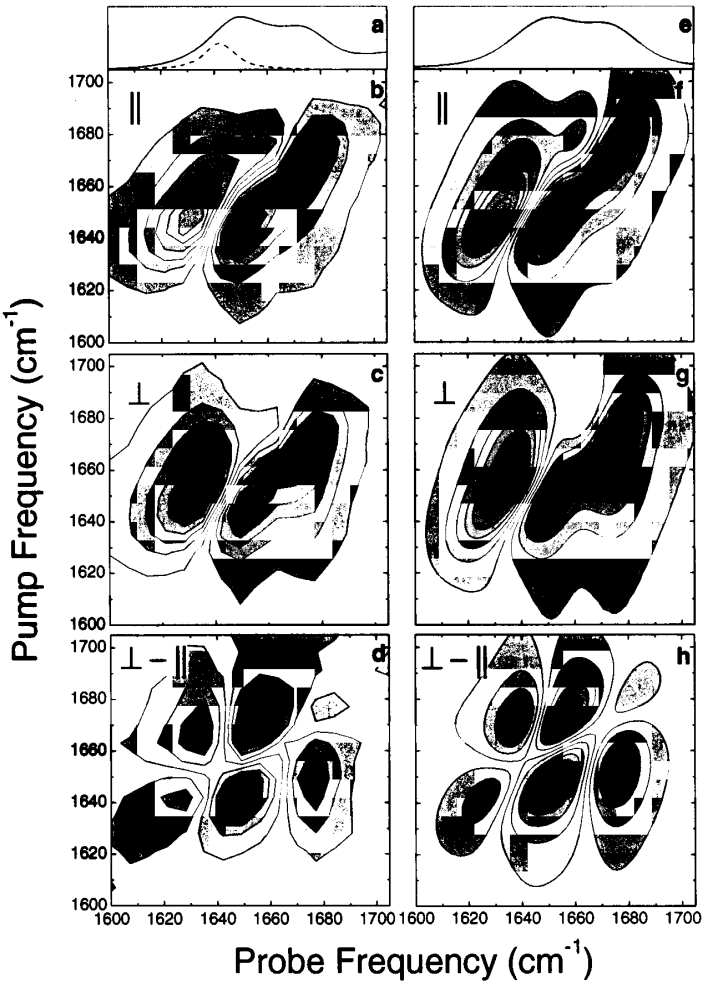

Figure 6. (a) Linear absorption spectrum of deuterated trialanine in D_2O at pD = 1. The dotted curve shows a representative pump-pulse spectrum. (b) 2D spectrum at delay 1.5 ps, for parallel polarizations of the pump and probe pulses, showing the absorption change as a function of pump and probe frequency. Blue colours indicate negative absorption change, red colours positive absorption change. Contour intervals are 0.13 mOD. (c) 2D spectrum for perpendicularly polarized pump and probe. Contour intervals are 0.05 mOD. (d) Difference between perpendicular and parallel signals (both scaled to the maximum value occurring in the respective 2D scans). Contour intervals are 0.04 mOD. (e)–(h) Calculated signals, using parameter values $\beta_{12} = 6\ \mathrm{cm}^{-1}$ and $\theta = 106°$. Contour intervals in the 2D plots are the same as on the left. Adapted from [19].

$\langle \delta\beta_{12}(t)\delta\beta_{12}(0)\rangle = d^2 \exp(-t/\tau)$, we obtain for the relaxation rate

$$k = \frac{2(d/\hbar)^2\tau}{1 + (\Delta\epsilon/\hbar)^2\tau^2}. \tag{19}$$

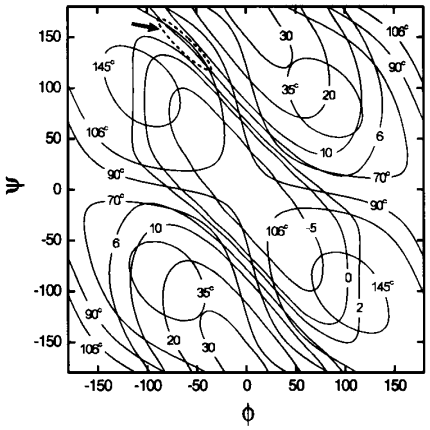

Figure 7. Calculated coupling strength β_{12} (in cm^{-1}, red contours), kindly provided to us by the authors of [88], and angle θ (in degrees, blue contours) between the two amide I transition dipoles as a function of the dihedral angles ϕ and ψ, which are defined as shown in figure 5. Adapted from [19].

The rate k has been determined experimentally for two values of $\Delta\epsilon$ using the Ala–Ala–Ala and Ala–Ala*–Ala samples, which are chemically identical, but have a different energy gap $\Delta\epsilon$ as a consequence of the ^{13}C isotope substitution. From the two k values we obtain the amplitude of the coupling correlation function $d = 5.2 \pm 0.5\ cm^{-1}$ and a correlation time $\tau = 110 \pm 20$ fs. Since the fluctuations in β_{12} directly mirror the fluctuations in the peptide dihedral angles (ϕ, ψ) [88], our measurements show that the conformation exhibits fluctuations which occur on a timescale of 100 fs.

It might seem surprising that a time constant of the order of 100 fs can be accurately determined using pump pulses which are several times longer (750 fs FWHM, see section 2.3). However, it should be noted that this time constant is not determined directly in a time-resolved pump–probe measurement, but derived (using equation (19)) from the two cross relaxation rates k, which are both very slow compared to the pump and probe pulse durations. In fact, it can be seen from equation (19) that the timescale to which the method presented here is most sensitive is given by the inverse of the frequency splitting between the coupled states, regardless of the duration of the pulses used in the experiment. The only requirement is that these durations be short enough to measure the cross relaxation rates from which the time constant is derived. It should be noted that the indirect determination of dynamical timescales which are much faster than the pulse duration is also widely used in NOESY spectroscopy [13].

It is instructive to compare our experimental results to the predictions obtained from the already mentioned MD simulation of trialanine in water [86]. Figure 10(A) shows a representative example of the calculated time evolution of the dihedral angles $\phi(t)$ and $\psi(t)$ pertaining to the central amino acid of trialanine (see figure 5). Figure 10(B) shows the instantaneous coupling $\beta_{12}(t)$, which was calculated from the (ϕ, ψ) trajectory with the aid of the *ab initio* based map of β_{12} as a function of (ϕ, ψ) (figure 7). Figure 10(C) shows the corresponding correlation function $\langle \delta\beta_{12}(t)\delta\beta_{12}(0)\rangle$, which is well approximated by a sum of two exponentially decaying components (shown as the red and green curves in figure 10(C)): an ultrafast inertial component with time constants $\tau_1 = 120$ fs and a fluctuation amplitude $d_1 = 4.1\ cm^{-1}$ and a slower, diffusive component with $\tau_2 = 2.2$ ps and $d_2 = 3.5\ cm^{-1}$.

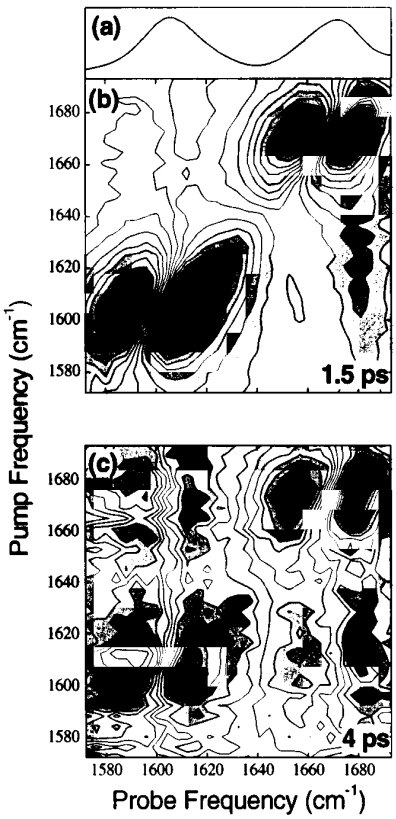

Figure 8. (a) Linear absorption spectrum of deuterated Ala–Ala*–Ala dissolved in D_2O. (b), (c) 2D spectra for perpendicular polarizations of the pump and probe pulses, showing the absorption change as a function of pump and probe frequency for mixing times of 1.5 ps (b) and 4 ps (c). Red denotes positive absorption change and blue denotes negative absorption change. The data have been scaled to eliminate the effect of T_1 relaxation. Adapted from [22].

From the MD data we can also calculate cross relaxation rates. We obtain values of 0.04 and 0.13 ps^{-1} for the cross relaxation rates of Ala–Ala*–Ala and Ala–Ala–Ala, respectively (insert of figure 10(C)), both reasonably close to the experimentally observed values. It can be seen from the insert of figure 10(C) that these rates are exclusively determined by the fast subpicosecond component of the correlation function (red curve), the time constant and amplitude of which agree well with the values derived from experiment (see table 1). Figures 10(A) and (C) show that this ultrafast component contributes significantly to the overall conformational dynamics of the peptide.

3.3. Distribution of conformations

Finally, we focus on the time dependence of the diagonal peaks (see figure 11). In the case of *N*-methylacetamide (NMA, CH_3–CONH–CH_3), a 'peptide monomer' used here as reference molecule, the pump–probe contours are tilted along the diagonal for short pump–probe delays (figure 11(b)). This means that the maximum absorption change occurs at a frequency which

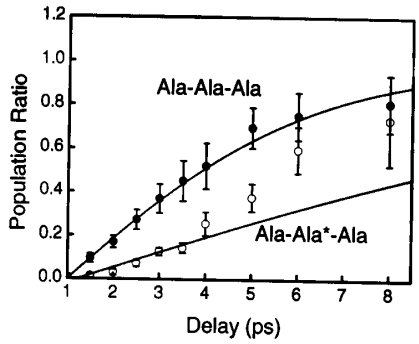

Figure 9. Population ratio as a function of mixing time for Ala–Ala*–Ala (open points) and Ala–Ala–Ala (full points), as obtained from the ratio of the cross and diagonal peaks observed in transient spectra recorded at different mixing times. The full curves represent fits to the data, with cross relaxation rates of 0.07 and 0.19 ps^{-1} for Ala–Ala*–Ala and Ala–Ala–Ala, respectively. Adapted from [22].

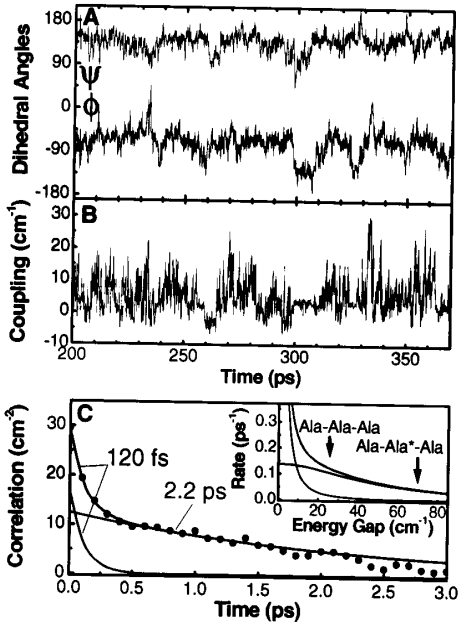

Figure 10. (A) Trajectory of the dihedral angles $\phi(t)$ and $\psi(t)$ of the central amino acid of trialanine as obtained from the MD simulation. (B) Instantaneous coupling $\beta_{12}(t)$ computed from the trajectory. (C) Coupling correlation function $\langle \delta\beta_{12}(t)\delta\beta_{12}(0)\rangle$, the Fourier transform of which determines the cross relaxation rate (insert). The arrows mark the frequency splittings of Ala–Ala–Ala and Ala–Ala*–Ala, respectively. The red and green curves represent the fast and slow components of the correlation function, respectively. Adapted from [22].

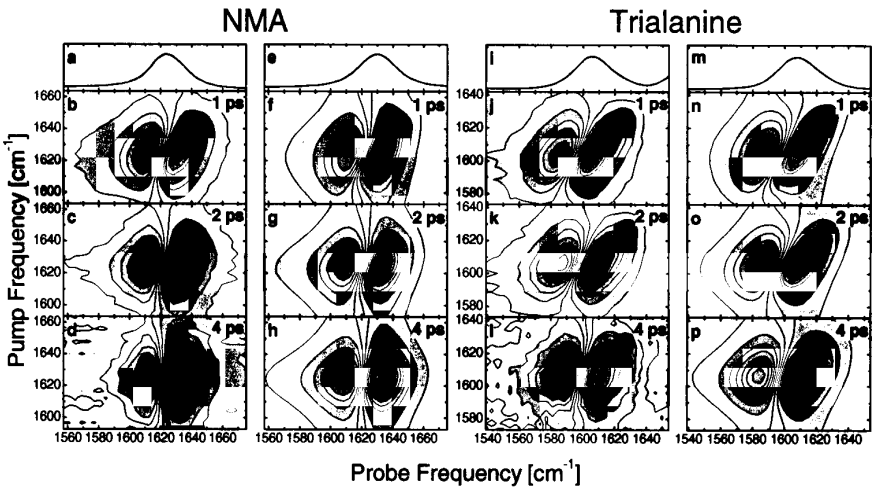

Figure 11. Linear and nonlinear amide I response of NMA and the centre amino acid of isotope-labelled trialanine Ala–Ala*–Ala. In the contour plots, blue colours indicate negative absorption change and red colours positive absorption change. The 2D spectra have been normalized to eliminate the overall decrease of the signal due to population relaxation. (a) Absorption spectrum of deuterated NMA in D_2O. (b)–(d) 2D pump–probe spectra of deuterated NMA, showing the absorption change as a function of pump and probe frequency at delays of 1 ps (b), 2 ps (c) and 4 ps (d). (e)–(h) Fitted absorption and 2D pump–probe spectra of NMA at delays of 1 ps (f), 2 ps (g) and 4 ps (h). (i) Absorption spectrum of deuterated Ala–Ala*–Ala in D_2O. (j)–(l) 2D pump–probe spectra of trialanine at delays of 1 ps (j), 2 ps (k) and 4 ps (l). (m)–(p) Fitted absorption and 2D spectra of trialanine at delay values of 1 ps. (n), 2 ps (o) and 4 ps (p). Adapted from [23].

Table 1. Comparison of experimental and MD results [22, 86] obtained for the peptide dihedral angles ϕ, ψ and the average transition coupling β_{12}, as well as for the correlation time τ and amplitude d of the cross relaxation correlation function.

	Structural parameters			Dynamical parameters	
	ϕ (deg)	ψ (deg)	β_{12} (cm^{-1})	τ (fs)	d (cm^{-1})
Experiment	−60	140	6	110 ± 20	5.2 ± 0.5
Theory	−68	141	5	120	4.1

varies with the pump frequency, implying that there exists a distribution of amide I frequencies, and that the narrow band pump pulse spectrally selects a specific subensemble (hole burning). The tilt of 2D diagonal peaks and its relation to inhomogeneous broadening has been discussed in detail before [45, 47, 57, 58]. With increasing mixing time τ_m, the contours become more vertically directed (figures 11(c) and (d)), i.e. the response of the system becomes less and less sensitive to the frequency at which it has been excited at $t = 0$. At a delay time of 4 ps, the contours have become completely vertically directed (figure 11(d)), which means that the observed absorption change has become independent of the pump frequency and that the random fluctuations of the transition frequency have completely washed out any memory about the initially selected sub-ensemble. *On the 4 ps timescale, the amide I band of NMA is homogeneous.*

The amide I band centre amino acid of isotope-labelled Ala–Ala*–Ala is shown in figure 11(i). The ^{13}C-isotope-labelling of the C=O group causes a large redshift of its amide I frequency, separating it from the other amide I bands. The pump–probe response of the amide I mode is shown in figures 11(j)–(l). At early delays, the response of the peptide C=O group is similar to that of the NMA C=O group but differs in one important respect: at 4 ps (figure 6(l)), there still exists significant inhomogeneity (the contours are still skewed), which means that spectral diffusion occurs on a sufficiently slow timescale that spectrally selected sub-ensembles can still be distinguished after 4 ps. In contrast to NMA, *the amide I band of trialanine is still notably inhomogeneous on the 4 ps timescale*. The lineshape functions of both transitions have been determined in [23] by fitting the experimental spectra (figures 11(e)–(h) and (m)–(p)).

The frequency fluctuation correlation function $\langle \delta\epsilon(t)\delta\epsilon(0)\rangle$ (see section 2.2) of the amide I mode reflects a superposition of various dynamical processes, which are difficult to separate. Since intermolecular hydrogen bonding of solvent water molecules and the peptide C=O group is known to cause a notable redshift of the amide I frequency, we have first studied the hydrogen-bonding dynamics of NMA and trialanine using MD simulations [23]. The calculated hydrogen bond lifetime of NMA was found to be of the same order as the measured spectral diffusion correlation time. Hence, we conclude that the lineshape function of NMA is dominated by hydrogen bond dynamics. Since the MD simulations predict quite similar timescales of hydrogen bonding for both NMA and trialanine, however, hydrogen bonding cannot be responsible for their distinctly different spectral response, namely the slow spectral diffusion process observed in trialanine.

In contrast to NMA, which contains only a single peptide unit, trialanine may exhibit conformational dynamics due to the highly flexible intramolecular degrees of freedom (ϕ, ψ) of the peptide bond. A quantum-chemical study has shown that the amide I frequencies of trialanine vary significantly with the central (ϕ, ψ) dihedral angles (a 'chemical shift') [23]. Hence, conformational fluctuations as well as transitions between various conformations are expected to contribute considerably to the overall frequency fluctuations of the transition. It turns out that the slow spectral diffusion observed in trialanine can be well explained by assuming that a small fraction of the molecules is in a conformation different from the dominant P_{II} one. MD simulations using the GROMOS96 force field predict three main peaks of the conformational distribution, the P_{II} conformation $(\phi, \psi) \approx (-67°, 132°)$, the β conformation $(\phi, \psi) \approx (-122°, 130°)$ and the α_R conformations $(\phi, \psi) \approx (-76°, -44°)$ [86, 89]. Due to the well-known uncertainty in the conformational population probabilities, the relative populations of these conformer states have to be determined by comparison with experimental data. From NMR experiments, we have found the ^3J-coupling between the C_α and the N proton to be 5.27 Hz [23], from which we obtain $\phi = -69°$ [90]. This angle is in agreement with both the P_{II} and α_R conformations, which have roughly the same ϕ dihedral angle, but excludes the β conformation. Both our 2D-IR experiments [19, 20] and IR/polarized Raman studies [91] strongly favour the P_{II} conformation. However, it is still possible that some of the molecules are in the α_R conformation. By combining the results of the MD simulations with an accurate analysis of the 1D and 2D lineshapes (see figures 11(m)–(p) and [23]), we have found that trialanine occurs predominantly (≈80%) in the P_{II} conformation and occasionally (≈20%) in the α_R-conformation.

4. Other vibrational spectroscopic methods

There exist several other spectroscopic methods which use (couplings between) molecular vibrations with the purpose of probing the conformations of peptides and proteins in solution. The most commonly used are conventional (linear) IR and Raman spectroscopy, VCD and Raman optical activity (ROA).

Until recently, the IR and Raman spectra of proteins and peptides were mainly used to derive general properties of the conformation by means of empirical rules, which were derived by measuring and comparing the IR spectra of a large number of proteins and peptides with known secondary structures. A well-known rule is the assignment of β-sheet and α-helical motifs to different frequency regions of the amide I band structure [92]. Another example is the empirical relations between the dihedral angles and the frequency of the amide III mode of a single peptide unit [93, 94], which might to some extent be used to derive the dihedral angles of the peptide unit from the IR spectrum.

The more recently developed methods of VCD and ROA both combine sensitivity to optical activity with the chemical bond specificity of vibrational spectroscopy. In VCD, one measures the vibrational optical activity by recording difference spectra of the IR absorption of left and right circularly polarized radiation [81]. In ROA, one measures the optical activity by recording the difference in the intensity of Raman scattering of right and left circularly polarized light [95]. Both the VCD and ROA spectra are more conformation-sensitive than conventional IR and Raman spectra due to the fact that mainly the normal modes which sample the skeletal chirality most directly contribute to the VCD and ROA intensity. As a consequence, ROA spectra of proteins contain distinct bands corresponding to different structural motifs.

Semi-empirical normal-mode calculations have long since been used to obtain a more detailed and quantitative understanding of the relation between secondary structure and the linear vibrational response measured in the techniques described above. By fitting of calculated to experimental spectra, the force-field parameters have been extensively optimized and, as a result, it is now possible to predict complete vibrational spectra from a known secondary peptide structure with reasonable accuracy [53]. More recently, density-functional theory calculations have been used to reproduce IR and Raman as well as VCD [96] spectra in an *ab initio* way. Although such semi-empirical and quantum-mechanical calculations can nowadays reproduce the observed spectra very well, it is clear that with such an approach it will generally not be possible to systematically *derive* the molecular conformation from the experimental linear spectra.

The results presented in section 3.1 suggest that such a structure elucidation does become possible by measuring the vibrational couplings and relative transition dipole angles in the molecule. The problem is that in general these couplings cannot be determined from the linear IR spectrum alone. Even for the smallest system consisting of two coupled amide I modes, there are four unknowns (ϵ_1, ϵ_2, β_{12}, and the angle θ_{12} between the transition dipoles) and three knowns in a linear IR spectrum (the frequencies of the two amide I bands and their relative intensity).

However, when combining linear IR spectra with conventional isotropic and anisotropic Raman spectroscopy, which as a nonlinear spectroscopy is capable of measuring intramolecular angles, it has been shown that it is in fact possible to determine all four unknowns (ϵ_1, ϵ_2, β_{12} and the angle θ_{12}) [91]. In more recent work, it has furthermore been suggested that one can determine the structure of a tripeptide even without using any model for the coupling constant β_{12}, by measuring two independent angles, namely the angle between the IR transition dipoles and the angle between the Raman tensor's principal axes [97].

5. Outlook

The methods presented here provide an unique way of investigating conformation and ultrafast conformational dynamics of small peptides. To our knowledge, our studies [19, 20, 22, 23], combined with [87, 91, 97], provide the most detailed experimental information to date on the conformation, conformational distribution and conformational dynamics of a small protein

building block. NMR spectroscopy essentially fails for such small systems due to their high flexibility and the lack of expressive NOESY peaks [98].

Only recently, NMR experiments in partially oriented samples of AcAlaMHMe, the central structure of which is identical to trialanine, have revealed essentially the same P_{II} conformation [99]. The same has been shown for Ala_7 [100]. In contrast to common belief, tripeptides may adopt rather well defined structures in solution, even though they cannot be stabilized by intramolecular hydrogen bonds. Interestingly for trialanine this structure is a stretched P_{II} conformation, which might explain the preference of this conformation in un- or mis-folded proteins [101]. Different MD force fields yield considerably different results for the conformational distribution of this type of model system [89, 102], even though one would hope to be able to reproduce the conformation of the smallest building blocks correctly before trying to predict protein structures. We therefore hope that our results will stimulate further refinement of MD force fields.

2D-IR spectroscopy has recently been extended to larger peptides such as small α-helices [21] and β-peptides [24]. However, 2D-IR spectroscopy will develop its real power only in combination with site-specific isotope labelling [103], separating one or two specific peptide units from the otherwise unresolved amide I band. The cross peak intensities and anisotropies can be used to determine the angles and couplings between each pair of amide I modes, and from these the (time-averaged) conformation of the peptide can be derived. Fluctuations of the conformation can be observed from time-resolved 2D-IR spectra. The cross relaxation between each pair of amide I modes will specifically mirror the fluctuations of those conformational degrees of freedom which determine the strength of the coupling between these two modes. In this way, it is possible to obtain a detailed, mode-specific picture of the subpicosecond conformational dynamics of the peptide or protein under study.

As yet, 2D-IR studies have focused only on the equilibrium states of peptides. The subpicosecond time resolution of 2D-IR spectroscopy makes it a powerful tool to also study the (fast) evolution of non-equilibrium states. In such 2D-IR experiments, the non-equilibrium state can be prepared using a short laser pulse (nanoseconds or less), and the subsequent evolution of the peptide conformation to the new equilibrium state probed by recording 2D-IR spectra at different delays with respect to the preparation pulse. A biologically relevant example is the formation and breaking up of α-helices, which is known to take place on a timescale of nanoseconds [104], well out of the range of NMR methods. The feasibility of time-resolved non-equilibrium experiments has already been demonstrated for time-delayed 1D probing, using either a heating pulse to initiate formation of the coil state [104, 105] or an optically triggered molecular switch directly incorporated into the peptide backbone [106–109]. With 2D-IR probing, it will be possible to follow the conformational changes involved in these processes in much more detail than with 1D methods [32].

Acknowledgments

PH wishes to thank Robin Hochstrasser for the interesting and most stimulating time in his laboratory, where the work described in this review had its origin. We also wish to thank Gerhard Stock and his co-workers for many inspiring and stimulating discussions, and Andrei Tokmakoff for sending us figure 4. Financial support by the Deutsche Forschungsgemeinschaft (DFG) and the Nederlandse Organisatie voor Wetenschappelijk Onderzoek (NWO) is greatly acknowledged. Most of the work was performed at and with the financial support of the Max Born Institute, Berlin, Germany. We gratefully thank Thomas Elsaesser for continued support of the project.

References

[1] Helliwell J R and P M R (ed) 1997 *Time Resolved Diffraction* (Oxford: Clarendon)
[2] Srajer V, Teng T, Ursby T, Pradervand C, Ren Z, Adachi S, Schildkamp W, Bourgeois D, Wulff M and Moffat K 1996 *Science* **274** 1726
[3] Ren Z, Bourgeois D, Helliwell J R, Moffat K, Srajer V and Stoddard B L 1999 *J. Synchrotron Rad.* **6** 891
[4] Techert S, Schotte F and Wulff M 2001 *Phys. Rev. Lett.* **86** 2030
[5] Neutze R, Wouts R, Techert S, Davidsson J, Kocsis M, Kirrander A, Schotte F and Wulff M 2001 *Phys. Rev. Lett.* **87** 195508
[6] Wüthrich K 1986 *NMR of Proteins and Nucleic Acids* (New York: Wiley-Interscience)
[7] Wüthrich K 1998 *Nat. Struct. Biol. Sci.* **5** 492
[8] Carrington A and McLachlan A D 1967 *Introduction to Magnetic Resonance* (New York: Harper & Row)
[9] Ernst R R, Bodenhausen G and Wokaun A 1987 *Principles of Nuclear Magnetic Resonance in One and Two Dimensions* (Oxford: Clarendon)
[10] Balbach J, Forge V, Lau W S, van Nuland N A J, Brew K and Dobson C M 1996 *Science* **274** 1161
[11] Winder P J H S L, Roberts C H and Dobson C M 1997 *J. Am. Chem. Soc.* **119** 5049
[12] Dobson C M and Hore P J 1998 *Nat. Struct. Biol. Sci.* **5** 504
[13] Lipari G and Szabo A 1982 *J. Am. Chem. Soc.* **104** 4546
[14] Mayo K H, Daragan V A, Idiyatullin D and Nesmelova I 2000 *J. Magn. Reson.* **146** 188
[15] Hamm P, Lim M and Hochstrasser R M 1998 *J. Phys. Chem.* B **102** 6123
[16] Hamm P, Lim M, DeGrado W F and Hochstrasser R M 1999 *Proc. Natl Acad. Sci. USA* **96** 2036
[17] Hamm P, Lim M, DeGrado W F and Hochstrasser R M 2000 *J. Chem. Phys.* **112** 1907
[18] Hamm P and Hochstrasser R M 2001 *Ultrafast Infrared and Raman Spectroscopy* ed M D Fayer (New York: Dekker) pp 273–347
[19] Woutersen S and Hamm P 2000 *J. Phys. Chem.* B **104** 11 316
[20] Woutersen S and Hamm P 2001 *J. Chem. Phys.* **114** 2727
[21] Woutersen S and Hamm P 2001 *J. Chem. Phys.* **115** 7737
[22] Woutersen S, Mu Y, Stock G and Hamm P 2001 *Proc. Natl Acad. Sci. USA* **98** 11 254
[23] Woutersen S, Pfister R, Hamm P, Mu Y, Kosov D S and Stock G 2002 *J. Chem. Phys.* at press
[24] Hamm P, Woutersen S and Rueping M 2002 *Helv. Chim. Acta* at press
[25] Asplund M C, Zanni M T and Hochstrasser R M 2000 *Proc. Natl Acad. Sci. USA* **97** 8219
[26] Zanni M T, Asplund M C and Hochstrasser R M 2001 *J. Chem. Phys.* **114** 4579
[27] Zanni M T, Ge N H, Kim Y S and Hochstrasser R M 2001 *Proc. Natl Acad. Sci. USA* **98** 11 265
[28] Chernyak V, Zhang W M and Mukamel S 1998 *J. Chem. Phys.* **109** 9587
[29] Zhang W M, Meier T, Chernyak V and Mukamel S 1998 *J. Chem. Phys.* **108** 7763
[30] Piryatinski A, Tretiak S, Chernyak V and Mukamel S 2000 *J. Raman Spectrosc.* **31** 125
[31] Scheurer C and Mukamel S 2001 *J. Chem. Phys.* **115** 4989
[32] Scheurer C and Mukamel S 2001 *J. Am. Chem. Soc.* **123** 3114
[33] Mukamel S 2000 *Annu. Rev. Phys. Chem.* **51** 691
[34] Golonzka O, Khalil M, Demirdöven N and Tokmakoff A 2001 *Phys. Rev. Lett.* **86** 2154
[35] Golonzka O, Khalil M, Demirdöven N and Tokmakoff A 2001 *J. Chem. Phys.* **115** 10 814
[36] Khalil M and Tokmakoff A 2001 *Chem. Phys.* **266** 213
[37] Torii H and Tasumi M 1992 *J. Chem. Phys.* **96** 3379
[38] Torii H and Tasumi M 1992 *J. Chem. Phys.* **97** 86
[39] Torii H and Tasumi M 1992 *J. Chem. Phys.* **97** 92
[40] Davidov A S 1971 *Theory of Molecular Excitons* (New York: Plenum)
[41] Bright Wilson E Jr, Decius J C and Cross P C 1955 *Molecular Vibrations* (New York: McGraw-Hill)
[42] Herzberg G 1945 *Molecular Spectra and Molecular Structure. II Infrared and Raman Spectra of Polyatomic Molecules* (New York: Van Nostrand-Reinhold)
[43] Mukamel S 1995 *Principles of Nonlinear Optical Spectroscopy* (Oxford: Oxford University Press)
[44] Gallagher Faeder S M, Albrecht A W, Hybl J D, Landin B L, Rajaram B and Jonas D M 1998 *J. Opt. Soc. Am.* B **15** 2338
[45] Hybl J D, Albrecht A W, Faeder S M G and Jonas D M 1998 *Chem. Phys. Lett.* **297** 307
[46] Gallagher Faeder S M and Jonas D M 1999 *J. Phys. Chem.* A **103** 10 489
[47] Hybl J D, Christophe Y and Jonas D M 2001 *Chem. Phys.* **266** 295
[48] Mills I M and Robiette A G 1985 *Mol. Phys.* **56** 743

[49] Nielsen H H 1951 *Rev. Mod. Phys.* **23** 90
[50] Pliva J 1990 *J. Mol. Spectrosc.* **139** 278
[51] Willetts A and Handy N C 1995 *Chem. Phys. Lett.* **235** 286
[52] Maslen P E, Jayatilaka D, Amos R D and Handy N C 1991 *J. Chem. Phys.* **95** 7409
[53] Krimm S and Bandekar J 1986 *Adv. Protein Chem.* **38** 181
[54] Hamm P and Woutersen S 2002 *Bull. Chem. Soc. Japan* **75** 985
[55] Kubo R, Toda M and Hashitsume N 1985 *Statistical Physics II. Nonequilibrium Statistical Mechanics* (Berlin: Springer)
[56] Hamm P, Lim M and Hochstrasser R M 1998 *Phys. Rev. Lett.* **81** 5326
[57] Okumura K, Tokmakoff A and Tanimura Y 1999 *Chem. Phys. Lett.* **314** 488
[58] Tokmakoff A 2000 *J. Phys. Chem.* A **104** 4247
[59] Fleming G R and Cho M 1996 *Annu. Rev. Phys. Chem.* **47** 109
[60] Mukamel S and Tanimura Y 1993 *J. Chem. Phys.* **99** 9496
[61] Okumura K and Tanimura Y 1998 *J. Opt. Soc. Am.* B **295** 298
[62] Cho M 2002 *Phys. Chem. Commun.* **7** 1
[63] Tominaga K and Yoshihara K 1995 *Phys. Rev. Lett.* **74** 3061
[64] Steffen T and Duppen K 1996 *Phys. Rev. Lett.* **76** 1224
[65] Tokmakoff A, Lang M J, Larsen D S, Fleming G R, Chernyak V and Mukamel S 1997 *Phys. Rev. Lett.* **79** 2702
[66] Blank D A, Kaufman L J and Fleming G R 2000 *J. Chem. Phys.* **113** 771
[67] Astinov V, Kubarych K J, Milne C J and Miller R J D 2000 *Chem. Phys. Lett.* **327** 334
[68] Zhao W and Wright J C 2000 *Phys. Rev. Lett.* **84** 1411
[69] Keusters D, Tan H-S and Warren W S 1999 *J. Phys. Chem.* A **103** 10369
[70] Hamm P, Kaindl R A and Stenger J 2000 *Opt. Lett.* **25** 1798
[71] DeSilvestri S, Weiner A M, Fujimoto J G and Ippen E P 1984 *Chem. Phys. Lett.* **112** 195
[72] Joo T and Albrecht A C 1993 *Chem. Phys. Lett.* **176** 233
[73] Cho M, Yu J Y, Joo T, Nagasawa Y, Passino S A and Fleming G R 1996 *J. Phys. Chem.* **100** 11944
[74] Joo T, Jia Y, Yu J-Y, Lang M J and Fleming G R 1996 *J. Phys. Chem.* **104** 6089
[75] Emde M F, Baltuška A, Kummrow A, Pshenichnikov M S and Wiersma D A 1998 *Phys. Rev. Lett.* **80** 4645
[76] Lim M, Hamm P and Hochstrasser R M 1998 *Proc. Natl Acad. Sci. USA* **95** 15315
[77] Levenson M D and Kano S S 1988 *Introduction to Nonlinear Laser Spectroscopy* (San Diego, CA: Academic)
[78] Goodno G D, Dadusc G and Miller R J D 1998 *J. Opt. Soc. Am.* B **15** 1791
[79] Astinov V, Kubarych K J, Milne C J and Miller R J D 2000 *Opt. Lett.* **25** 853
[80] Emde M F, de Boeij W P, Pshenichnikov M S and Wiersma D A 1997 *Opt. Lett.* **22** 1338
[81] Lee O, Roberts M and Diem M 1989 *Biopolymers* **28** 1759
[82] Zuk W M, Freedman T B and Nafie L A 1989 *Biopolymers* **28** 2025
[83] Ford S J, Wen Z Q, Hecht L and Barron L D 1994 *Biopolymers* **34** 303
[84] Press W H, Teukolsky S A, Vetterling W T and Flannery B P 1992 *Numerical Recipes in C* (Cambridge: Cambridge University Press)
[85] Creighton T E 1993 *Proteins* (New York: Freeman)
[86] Mu Y and Stock G 2002 *J. Phys. Chem.* B **106** 5294
[87] Dorai K and Griesinger C 2002 unpublished results
[88] Torii H and Tasumi M 1998 *J. Raman Spectrosc.* **29** 81
[89] Mu Y, Kosov D S and Stock G 2002 *J. Chem. Phys.* submitted
[90] Karplus M J 1959 *J. Chem. Phys.* **30** 11
[91] Schweitzer-Stenner Q H R, Eker F and Griebenov K 2001 *J. Am. Chem. Soc.* **123** 9628
[92] Surewicz W K and Mantsch H H 1993 *Biochemistry* **32** 389
[93] Lord R C 1977 *Appl. Spectrosc.* **31** 187
[94] Ianoul A, Boyden M N and Asher S A 2001 *J. Am. Chem. Soc.* **123** 7433
[95] Barron L D 2000 *Prog. Biophys. Mol. Biol.* **73** 1
[96] Kubelka J and Keiderling T A 2001 *J. Am. Chem. Soc.* **123** 12048
[97] Schweitzer-Stenner R 2002 *Biophys. J.* **83** 523
[98] Madison V and Kopple K D 1980 *J. Am. Chem. Soc.* **102** 4855
[99] Poon C-D, Samulski E T, Weise C F and Weisshaar J C 2000 *J. Am. Chem. Soc.* **122** 5642
[100] Shi Z, Olson C A, Rose G D, Baldwin R L and Kallenbach N R 2002 *Proc. Natl Acad. Sci. USA* **99** 9190
[101] Shi Z, Woody R W and Kallenbach N R 2002 *Adv. Protein Chem.* at press
[102] Hu H and Hermans J 2002 *Proteins* at press

[103] Ludlam C F C, Arkin I T, Rothman M S, Rath P, Aimoto S, Smith S O, Engelman D M and Rothschild K J 1996 *Biophys. J.* **70** 1728
[104] Thompson P A, Eaton W A and Hofrichter J 1997 *Biochemistry* **36** 9200
[105] Williams S, Causgrove T P, Gilmanshin R, Fang K S, Callender R H, Woodruff W H and Dyer R B 1996 *Biochemistry* **35** 691
[106] Volk M, Kholodenko Y, Lu H S M, Gooding E A, WF W F D and Hochstrasser R M 1997 *J. Phys. Chem.* B **101** 8607
[107] Renner C, Behrendt R, Sporlein S, Wachtveitl J and Moroder L 2000 *Biopolymers* **54** 489
[108] Spörlein S, Carstens H, Renner H S C, Behrendt R, Moroder L, Tavan P, Zinth W and Wachtveitl J 2002 *Proc. Natl Acad. Sci. USA* **99** 7998
[109] Bredenbeck J, Helbing J, Sieg A, Schrader T, Zinth W, Wachtveitl J, Renner C, Behrendt R, Moroder L and Hamm P 2002 submitted